

Ultrasensitive Magnetometers Based on Carbon-Nanotube Mechanical Resonators

B. Lassagne,* D. Ugnati, and M. Respaud

Université de Toulouse, Laboratoire de Physique et Chimie des Nano-Objets (LPCNO CNRS-INSA-UPS), UMR 5215, Toulouse, France

(Received 11 March 2011; revised manuscript received 19 July 2011; published 23 September 2011)

We describe herein how a nanoelectromechanical system based on a carbon nanotube used as a force sensor can enable one to assess the magnetic properties of a single and very small nano-object grafted onto the nanotube. Numerical simulations performed within the framework of the Euler-Bernoulli theory of beams predict that the magnetic field dependence of the nanotube mechanical resonance frequency is a direct probe for the nano-object magnetic properties and that a sensitivity around a few (few hundreds) Bohr magnetic moments at low temperature (room temperature) can be expected.

DOI: 10.1103/PhysRevLett.107.130801

PACS numbers: 07.55.Jg, 81.07.De, 81.07.Oj, 85.85.+j

Recent progresses in nanofabrication have enabled production of promising carbon-nanotube nanoelectromechanical systems (CNTNEMS). Such devices are made by suspending over a trench etched in a SiO_2/Si wafer a single wall carbon nanotube between two metallic electrodes [Fig. 1(a)]. The nanotube is actuated by means of the electrostatic interaction between the Si back gate and the nanotube. The mechanical motion is detected by measuring with a mixing technique the mechanically induced modulation of the electronic current passing through the CNTNEMS [1]. These devices are now well mastered and can operate between very low and room temperature and likely under any magnetic field conditions [1–7]. CNTNEMS are exceptional tools for ultrasensitive measurements. Their potential as sensors was first experimentally demonstrated by measuring their outstanding mass sensitivity in the range of a few atoms at low temperature (4 K) [2–4]. Such sensitivity results from the exceptional mechanical properties of carbon nanotubes, their large Young modulus, and their small radius (≈ 1 nm), which enables the reduction of the sensor mass down to the attogram. It also suggests that large force sensitivity could be reached because the stiffness k of a beam decreases with its radius r ($k \propto r^4$). Furthermore, CNTNEMS can easily enter in a nonlinear mechanical regime, even at low excitation voltage. As demonstrated recently, such nonlinear behavior can be very useful to enhance the sensitivity of CNTNEMS-based sensors [6,8].

Among the numerous potential sensing applications of CNTNEMS, we propose to use them as ultrasensitive magnetometers for the magnetic hysteresis measurements of a very small individual magnetic nano-object (NO). The principle of magnetic sensing with a CNTNEMS is based on torque magnetometry. The NO to study which is characterized by a magnetic moment m and a magnetic anisotropy energy K is rigidly grafted onto a CNTNEMS [Fig. 1(a)]. When a magnetic field B is applied, m undergoes a magnetic torque $\vec{\Gamma}_{\text{mag}} = \vec{m} \times \vec{B}$ which causes its rotation towards the magnetic field direction [Fig. 1(b)].

Then the NO rotates in order to minimize the magnetic anisotropy energy and causes the CNTNEMS to bend [Fig. 1(b)]. Thus, the mechanical tension inside the CNTNEMS increases and its mechanical resonance frequency is shifted. This frequency shift can be detected by measuring the CNTNEMS mechanical resonance frequency both when no magnetic field is applied and when a magnetic field is applied.

We show in this Letter that the magnetic field dependence of the mechanical resonance frequency is a unique signature of the NO magnetic properties. Our calculations performed within the framework of the Euler-Bernoulli theory of beams [9] enable the estimation of the mechanical resonance frequency versus the applied magnetic field, its direction, and its magnitude, and in turn the CNTNEMS sensitivity. For the sake of simplicity, we will consider a NO with a uniaxial magnetic anisotropy characterized by its direction c and its energy K [Fig. 1(b)]. The NO magnetic moment behaves according to the Stoner and

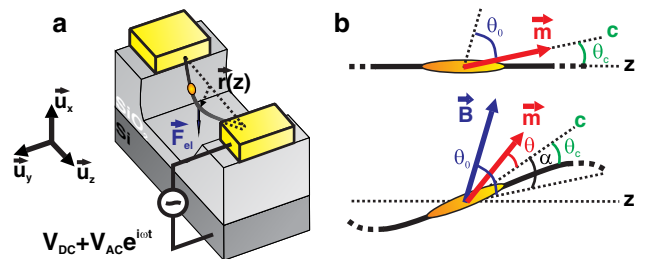


FIG. 1 (color online). (a) Schematic view of a CNTNEMS. A single wall carbon nanotube is suspended between two metallic electrodes over a trench etched in a SiO_2/Si wafer. The potential $V_{\text{DC}} + V_{\text{AC}}e^{i\omega t}$ actuates the nanotube. $r(z)$ is the CNTNEMS motion in the basis (x, y, z) . (b) Schematic view of a magnetic NO (represented in orange) grafted onto the CNTNEMS. θ_c is the angle between the NO anisotropy axis c and the CNTNEMS. θ_0 is the angle made by the magnetic field with regard to the c axis at zero magnetic field, θ is the angle between m and c , and α is the bending angle of the nanotube under magnetic field.

Wohlfarth model [10]. Magnetic field dependence of the frequency curves is calculated for different magnetic field orientations. Interestingly, their shapes reflect the main magnetic hysteresis curve characteristics. By optimizing the NO position, sensitivities around a few Bohr magnetic moments (μ_B) are expected with the state of the art CNTNEMS properties.

To determine quantitatively the magnetic field dependence of the CNTNEMS mechanical resonance frequency, we solve by using finite difference methods the Euler-Bernoulli equation of motion, which reads

$$\begin{aligned} EI \frac{\partial^4 \vec{r}(z, t)}{\partial z^4} - T \frac{\partial^2 \vec{r}(z, t)}{\partial z^2} + \eta \frac{\partial \vec{r}(z, t)}{\partial t} - \vec{F}_{\text{el}} - \vec{F}_{\text{mag}} \\ = -[\rho \pi d + m_{\text{NO}} \delta(z - z_0)] \frac{\partial^2 \vec{r}(z, t)}{\partial t^2} \end{aligned} \quad (1)$$

with $\vec{r}(z, t)$ the amplitude of motion as a function of the time t and the position z along the nanotube [Fig. 1(a)], E the Young modulus, d and L the nanotube diameter and length, respectively, $I = \frac{\pi d^4}{64}$ the quadratic moment for a cylinder beam, T the induced mechanical tension, ρ the graphene density in kg m^{-2} , m_{NO} and z_0 the NO mass and position, respectively, and η the damping coefficient per unity of length responsible for the mechanical energy losses. The electrostatic force \vec{F}_{el} actuating the nanotube reads $\vec{F}_{\text{el}} \approx \frac{1}{2} [C'_g V_{\text{DC}}^2 + C'_g V_{\text{DC}} V_{\text{AC}} e^{i\omega t}] \vec{u}_x$ with C'_g the derivative of the gate capacitance with respect to the distance between the Si back gate and the CNTNEMS. V_{DC} is the static voltage and V_{AC} the oscillating voltage applied on the back gate such as $V_{\text{AC}} \ll V_{\text{DC}}$. \vec{F}_{mag} is the force induced by the magnetic field on the CNTNEMS. It is related to the magnetic torque undergone by the NO. As explained in the introduction, when B is applied along a direction θ_0 with respect to c , m rotates by an angle θ to minimize the total NO magnetic energy $E_{\text{mag}} = E_z + E_K = -mB \cos(\theta_0 - \theta - \alpha) + K \sin^2(\theta)$. E_z is the Zeeman energy and E_K the magnetic anisotropy energy responsible of the mechanical coupling between the magnetic moment direction and the NO orientation. Because of this coupling, the magnetic torque $\Gamma_{\text{mag}} = -\frac{dE_z}{d\theta} = mB \sin(\theta_0 - \theta - \alpha)$ is mechanically transferred to the CNTNEMS and causes the CNT to bend by an angle α [Fig. 1(b)]. Note that we consider the NO is rigidly coupled to the CNTNEMS which means that the c axis keeps its orientation with regard to the nanotube axis during the magnetic moment rotation. This hypothesis is fairly justified by the fact that E_K is in the range of a few meV, therefore well below the adhesion work of a few eV [11] of a NO onto the nanotube or even the binding energy (in the eV range) of a functionalized NO which can form covalent bonds with the nanotube. Finally, we can model Γ_{mag} by the application of two forces $F_{\text{mag}} = \Gamma_{\text{mag}}/d_{\text{NO}}$ at

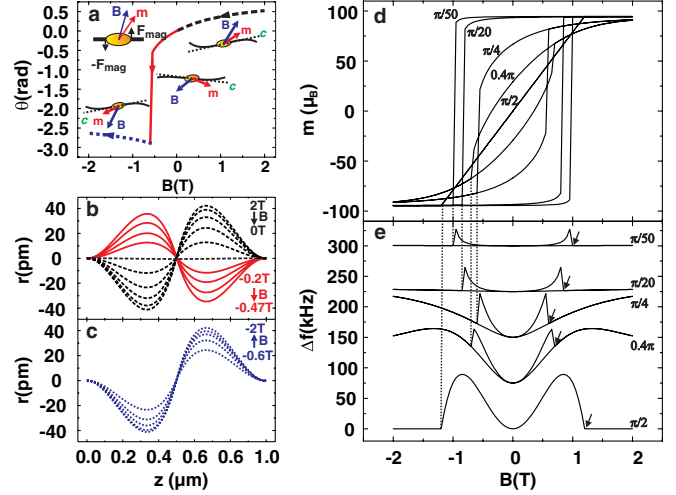


FIG. 2 (color online). Magnetic field dependence of the CNTNEMS mechanical properties and of θ . The magnetic field is in the (x, z) plane. (a) Magnetic field dependence of θ for $\theta_0 = \pi/4$. (b),(c) Shape of the CNTNEMS under magnetic field. The curve in the absence of a magnetic field shows a tiny negative bending due to the electrostatic force. The black dashed (red solid, purple dotted) curves correspond to the black dashed (red solid, purple dotted) curve in (a). (d),(e) Magnetic hysteresis loop of the NO and magnetic field dependence of the CNTNEMS mechanical resonance frequency for different θ_0 . For more clarity, the frequency curves are shifted by 75 kHz. The black arrows point to the field at which m jumps.

each edge of the NO [Fig. 2(a)] with d_{NO} the contact length between the NO and the CNT [12].

We investigate the CNTNEMS dynamical response in the case of a metallic iron NO having its anisotropy axis along the CNTNEMS ($\theta_c = 0$) and grafted at the middle of the CNTNEMS ($z_0 = L/2$). The magnetic field stays in the (x, z) plane, which is orthogonal to the substrate and makes an angle θ_0 with respect to the c axis (equivalent to the CNTNEMS axis in our example). The NO has a diameter d_{NO} of 1 nm ($m = 94.6\mu_B$) and a magnetic anisotropy energy $K = 3.3$ meV [13]. We simulate a realistic CNTNEMS having a $L = 1$ μm and a $d = 1$ nm in order to estimate the sensitivity of our device in real conditions. We used a C'_g of 10^{-14} F m^{-1} [14]. The simulations were performed at small V_{DC} , typically below 0.5 V (in Fig. 2, $V_{\text{DC}} = 50$ mV) in order for the magnetic torque induced bending to dominate the electrostatic bending. With values of V_{DC} higher than 1 V, the electrostatic bending decreases the magnetic torque effect (see [14] for the figure showing the electrostatic dependence of the magnetic torque effect). Figures 2(b) and 2(c) show the CNTNEMS shape versus the amplitude of a magnetic field applied along a fixed direction $\theta_0 = \pi/4$. As expected intuitively, the two forces F_{mag} lead to a symmetrical bending displaying an S shape. Figure 2(a) shows the evolution of the magnetic moment orientation θ as a function of B . We see that the coercive magnetic field is roughly 0.6 T. Thus, starting at $B = 2$ T,

where m is almost aligned with B , the S shape of the CNTNEMS has a maximum amplitude [black dashed curves in Fig. 2(b)] which is roughly 40 pm. By decreasing B , m tends to align with c (θ decreases), thus leading to the decreases of both F_{mag} and the amplitude of the bending [black dashed curves in Fig. 2(b)]. By reversing the magnetic field (between 0 and -0.6 T), m moves away from the c axis [red solid curves in Fig. 2(a)], which increases the bending [red solid curves in Fig. 2(b)]. At $B \approx -0.6$ T, m abruptly jumps from -0.31 (-31.5°) to -2.87 rad (-164.4°), thus leading to an abrupt inversion of F_{mag} and simultaneously of the CNTNEMS S shape when comparing Figs. 2(b) and 2(c). Then upon increasing B negatively, θ tends to $-3\pi/4$ and the maximum bending of the CNTNEMS reaches a limit value around 40 pm [see Fig. 2(c)]. The key point here is that the CNTNEMS bending follows the magnetic field dependence of the magnetic moment rotation and jumps at the same critical magnetic field.

From the bending of the CNTNEMS, we can calculate the mechanical resonance frequency shift. Figures 2(d) and 2(e), respectively, show the calculated magnetic hysteresis of the NO and the corresponding magnetic field dependence of the mechanical resonance frequency shift for different θ_0 . We observe that when m abruptly jumps, the frequency shift undergoes a discontinuity [pointed out by arrows, Fig. 2(e)], as a consequence of the abrupt change of the CNTNEMS shape. The same characteristic behavior occurs for any magnetic field orientation θ_0 . Hence, the CNTNEMS magnetometer can directly give the switching magnetic fields. Moreover, for each θ_0 value, a characteristic magnetic hysteresis loop corresponds to a unique mechanical resonance frequency hysteresis. Note also that the frequency shift is of the order of a few tenths of a kilohertz and reaches 90 kHz for a NO having a magnetic moment about $100\mu_B$. This shift would be easily detectable since it is much higher than the frequency noise of standard CNTNEMS (around a few kilohertz for a 1 Hz bandwidth at low temperature [3,5]). The frequency noise is the fundamental limitation of this technique. It can be caused by electrostatic fluctuations in the carbon nanotube, impurity pollution, or thermomechanical noise.

We now study the CNTNEMS magnetic sensitivity versus the NO position, keeping all the other parameters constant. Figure 3(a) shows the CNTNEMS bending for $\theta_0 = \pi/2$ and $B = 0.85$ T (where the frequency shift is maximum) for different NO positions. Figure 3(b) shows the corresponding mechanical resonance frequency as a function of the NO position. The frequency shift is maximal when the NO is grafted at $L/4$ (the shift is 2.2 times higher than at $L/2$). It corresponds to the maximum bending of the CNTNEMS [Fig. 3(a)]. Then numerical simulations with a NO having a smaller diameter $d_{\text{NO}} = 0.5$ nm ($m \approx 12\mu_B$) and the same anisotropy field were performed. Figure 3(d)

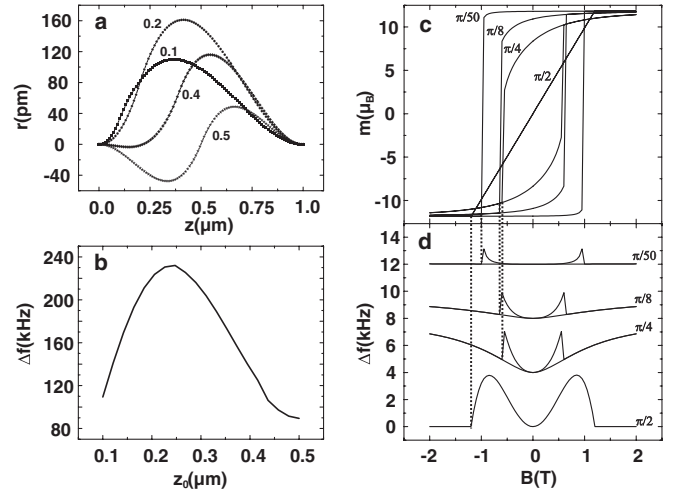


FIG. 3. Effect of the NO position on the CNTNEMS magnetic sensitivity. (a) Shape of the CNTNEMS as a function of z for different NO positions 0.1, 0.2, 0.4, and 0.5 μm . $d_{\text{NO}} = 1$ nm, $B = 0.85$ T, and $\theta_0 = \pi/2$. (b) Corresponding frequency shift. The maximum frequency shift is achieved near $L/4$. (c) Magnetic loop hysteresis of a NO with $d = 0.5$ nm. (d) CNTNEMS magnetic frequency shift dependency for different θ_0 with the NO grafted at $L/4$. The curves are shifted by 4 kHz for more clarity. The magnetic frequency shift ranges between 1 and 4 kHz.

shows the magnetic field dependence of the mechanical resonance frequency shift for 4 different values of θ_0 . The average frequency shift is now reduced between 2 and 4 kHz and compares with the frequency noise of the current CNTNEMS [5]. Hence, the sensitivity using state of the art devices would be around $12\mu_B$ in a 1 Hz bandwidth at low temperature. However, we can anticipate some improvements of the CNTNEMS performances; indeed, the sensitivity of a mechanical beam is ultimately limited by the thermomechanical fluctuations [15]. The lowest frequency noise δf_{th} achievable can be determined from $\delta f_{\text{th}} = \frac{1}{2\pi} \left(\frac{k_B T}{k x_0^2} \frac{2\pi f_0 W}{Q} \right)^{1/2}$ with k the stiffness constant, x_0 the amplitude of motion, f_0 the mechanical resonance frequency, W the measurement bandwidth, and Q the quality factor of the device [15]. Considering the very high Q value of 10^5 obtained recently [5] and a resonant frequency $f_0 = 50$ MHz for a CNTNEMS with a length of 1 μm , $k \approx 10^{-4}$ N m^{-1} , then a δf_{th} in the range of 50 Hz could be reached at 4 K for a 1 Hz bandwidth. Hence it would be reasonable to expect reaching the limit of $1\mu_B$ at low temperature by optimizing the devices. Nevertheless, very high sensitivities in the range of a few hundreds of μ_B can be anticipated over a broad range of magnetic field and up to room temperature with state of the art devices (Q is around 200 at 300 K and δf_{th} is around a few hundreds of a kilohertz for current devices [3]).

These simulations have been made in the particular configuration where the NO anisotropy axis c is along the nanotube axis and B is in the (x, z) plane. In this

case, B induces magnetic forces in the same plane as the electrostatic force. As long as the c axis remains in the (x, z) plane whatever the electrostatic force amplitude or magnetic field amplitude, the magnetic field dependence of the frequency shift and its amplitude behave identically. Otherwise, when the magnetic field is applied at any direction out of the (x, z) plane, the frequency shift behaves identically as long as the electrostatic bending is small compared to the magnetic bending. In the case of a strong initial electrostatic bending, the frequency shift becomes smaller because the magnetic forces appearing in the (x, z) plane tend to rigidify the CNTNEMS. Adding a lateral side gate can solve this latter problem. Finally, it is important to emphasize that, although the numerical simulations have been made with a metallic NO in the Stoner Wohlfarth regime, we can generalize our results to any kind of NO nature and regime. The CNTNEMS response would behave identically; each time the magnetic moment will jump, the frequency will present a discontinuity.

In conclusion, CNTNEMS-based magnetometry could constitute a new versatile and powerful approach comparable to or even better in theory than the existing ultrasensitive magnetometry techniques which are based on magnetotransport measurements [16–19], magnetic force or torque measurements [20–24], or magnetic flux measurements with a micro-SQUID [25]. Indeed, our numerical simulations allowed us to demonstrate that a CNTNEMS can directly probe the magnetic hysteresis loop of a very small anisotropic magnetic moment carried by a NO. Interestingly, the CNTNEMS may operate at a magnetic field of any amplitude and any direction, and they can reach theoretical sensitivities about a few (hundred) μ_B at low (room) temperature within a bandwidth of 1 Hz. It is in theory better than the best magnetometry techniques, the micro-SQUID, which has reached a sensitivity around $10^4 \mu_B$ in a 1 Hz bandwidth below 6 K [26]. We have to note that a sensitivity of a few μ_B is also expected with the nano-SQUID based on carbon nanotubes [27]. However, CNTNEMS would have the advantages to not be restricted at low temperature and moderate magnetic field. Thus, even though CNTNEMS deserve now experimental investigations to estimate their potential for magnetic sensing in realistic experimental conditions, we can anticipate that such devices could offer the possibility to investigate the magnetic properties of single NO independently of several distribution effects (size, shape, chemical distribution in nanoalloys, etc.) that are inherent to the chemical routes of synthesis. In the fields of molecular crystals such as the single molecule magnet, they could allow one to study numerous quantum effects ranging from quantum tunneling of magnetization to Berry phase interference and quantum coherence [28–30]. Magnetometry of such a kind of NO may have important consequences on the physics of spintronic devices or on numerous applications in the fields of magnetic biological applications

[31–33]. Finally, the most challenging hurdle to overcome before performing magnetometry with a CNTNEMS is the precise control of the grafting of a single NO onto the nanotube. Several deposition techniques have already been developed allowing the grafting of a few nanoparticles onto nanotubes [34,35]. Also, the technique of nanodispensing of a liquid by using a modified cantilever [36] could be used to achieve this goal.

The authors thank T. Blon, J. Carrey, L.-M. Lacroix, T. Ondarcuhu, and D.-G. Sanchez for fruitful discussions. This work was supported by the ANR 2010 JCJC 1003 1 “CARNAMAG,” the University of Toulouse, and Région Midi-Pyrénées in France.

*Corresponding author.

lassagne@insa-toulouse.fr

- [1] V. Sazonova *et al.*, *Nature* (London) **431**, 284 (2004).
- [2] K. Jensen *et al.*, *Nature Nanotech.* **3**, 533 (2008).
- [3] B. Lassagne *et al.*, *Nano Lett.* **8**, 3735 (2008).
- [4] H.-Y. Chiu *et al.*, *Nano Lett.* **8**, 4342 (2008).
- [5] A. K. Hüttel *et al.*, *Nano Lett.* **9**, 2547 (2009).
- [6] B. Lassagne *et al.*, *Science* **325**, 1107 (2009).
- [7] G. A. Steele *et al.*, *Science* **325**, 1103 (2009).
- [8] H. Cho *et al.*, *Nano Lett.* **10**, 1793 (2010).
- [9] A. N. Cleland, *Foundations of Nanomechanics: From Solid-State Theory to Device Applications* (Springer-Verlag, Berlin, 2003).
- [10] E. C. Stoner *et al.*, *Phil. Trans. R. Soc. A* **240**, 599 (1948).
- [11] Y. He *et al.*, *Appl. Phys. Lett.* **96**, 063108 (2010).
- [12] Note that as long as d_{NO} is less inferior than the length of the nanotube, it has no effect on the magnetic torque effect.
- [13] L.-M. Lacroix *et al.*, *J. Appl. Phys.* **103**, 07D521 (2008).
- [14] $C'_g \approx 10^{-14} \text{ F m}^{-1}$ allows one to fit with our model the mechanical resonance frequency gate voltage dependency of the experiments carried out in Ref. [3] (see Supplemental Material at <http://link.aps.org/supplemental/10.1103/PhysRevLett.107.130801> for the figure showing the fit).
- [15] K. L. Ekinci *et al.*, *J. Appl. Phys.* **95**, 2682 (2004).
- [16] S. Gueron, M. M. Deshmukh, E. B. Myers, and D. C. Ralph. *Phys. Rev. Lett.* **83**, 4148 (1999).
- [17] M. V. Rastei *et al.*, *Phys. Rev. Lett.* **99**, 246102 (2007).
- [18] A. Bernard-Mantel *et al.*, *Nature Phys.* **5**, 920 (2009).
- [19] A. Oral *et al.*, *Appl. Phys. Lett.* **69**, 1324 (1996).
- [20] J. P. Davis *et al.*, *Appl. Phys. Lett.* **96**, 072513 (2010).
- [21] C. Rossel *et al.*, *J. Appl. Phys.* **79**, 8166 (1996).
- [22] B. C. Stipe, H. J. Mamin, T. D. Stowe, T. W. Kenny, and D. Rugar, *Phys. Rev. Lett.* **86**, 2874 (2001).
- [23] D. Rugar *et al.*, *Nature* (London) **430**, 329 (2004).
- [24] G. de Loubens *et al.*, *Phys. Rev. Lett.* **98**, 127601 (2007).
- [25] M. Jamet *et al.*, *Phys. Rev. Lett.* **86**, 4676 (2001).
- [26] W. Wernsdorfer, *Supercond. Sci. Technol.* **22**, 064013 (2009).
- [27] J.-P. Cleuziou *et al.*, *Nature Nanotech.* **1**, 53 (2006).

-
- [28] L. Thomas *et al.*, *Nature (London)* **383**, 145 (1996).
[29] W. Wernsdorfer *et al.*, *Science* **284**, 133 (1999).
[30] A. Ardavan *et al.*, *Phys. Rev. Lett.* **98**, 057201 (2007).
[31] P. Seneor *et al.*, *J. Phys. Condens. Matter* **19**, 165222 (2007).
[32] L. Bogani *et al.*, *Nature Mater.* **7**, 179 (2008).
[33] Q.A. Pankhurst *et al.*, *J. Phys. D* **36**, R167 (2003).
[34] I. Rod *et al.*, *Nanotechnology* **20**, 335301 (2009).
[35] S. Mao *et al.*, *Nanotechnology* **19**, 455610 (2008).
[36] A. Fang *et al.*, *Nano Lett.* **6**, 2368 (2006).